

Imitation Learning with Stability and Safety Guarantees

He Yin, Peter Seiler, Ming Jin and Murat Arcak

Abstract—A method is presented to learn neural network (NN) controllers with stability and safety guarantees through imitation learning (IL). Convex stability and safety conditions are derived for linear time-invariant plant dynamics with NN controllers by merging Lyapunov theory with local quadratic constraints to bound the nonlinear activation functions in the NN. These conditions are incorporated in the IL process, which minimizes the IL loss, and maximizes the volume of the region of attraction associated with the NN controller simultaneously. An alternating direction method of multipliers based algorithm is proposed to solve the IL problem. The method is illustrated on an inverted pendulum system, aircraft longitudinal dynamics, and vehicle lateral dynamics.

I. INTRODUCTION

Imitation learning (IL) is a class of methods that learns a policy to attain a control goal consistent with expert demonstrations [1], [2]. Used in tandem with deep neural networks (NNs), IL presents unique advantages, including a substantial increase in sample efficiency compared to reinforcement learning (RL) [3], and wide applicability to domains where the reward model is not accessible or on-policy data is difficult/unsafe to acquire [1]. While IL is closely related to supervised learning as it trains a mapping from observations to actions [4], a key difference is the ensuing deployment of the learned policy under dynamics, which consequently raises the issue of closed-loop stability. This problem naturally falls within the realm of robust control, which analyzes stability for uncertain linear or nonlinear systems; however, a major technical challenge is to derive nonconservative guarantees for highly nonlinear policies such as NNs that can be also tractably incorporated into the learning process.

This letter tackles this issue and presents a method to learn NN controllers with stability and safety guarantees through IL. We first derive convex stability and safety conditions for linear time-invariant (LTI) plant dynamics by merging Lyapunov theory with local sector quadratic constraints (QCs) to describe the activation functions in the NN. Then we incorporate these constraints in the IL process that minimizes the IL loss, and maximizes the volume of the region of attraction associated with the NN controller. Finally, we propose an alternating direction method of multipliers (ADMM) based method to solve the IL problem.

Funded in part by the Air Force Office of Scientific Research grant FA9550-18-1-0253, the Office of Naval Research grant N00014-18-1-2209, and the U.S. National Science Foundation (NSF) grants ECCS-1906164. M. Jin acknowledges the funding from NSF EPCN-2034137.

H. Yin and M. Arcak are with the University of California, Berkeley {he_yin, arcak}@berkeley.edu.

P. Seiler is with the University of Michigan, Ann Arbor pseiler@umich.edu.

M. Jin is with the Virginia Tech jinming@vt.edu.

While there are many works focusing on NN robustness analysis using QCs, e.g., NN safety verification [5], NN Lipschitz constant estimation [6], reachability analysis [7] and stability analysis [8]–[10] of NN controlled systems, there are relatively fewer results regarding NN synthesis, including NN training with bounded Lipschitz constants [11], and recurrent NN training with bounded incremental ℓ_2 gains [12].

Compared to existing works, this letter makes the following contributions. First, it presents a safe IL algorithm to synthesize NN controllers, which trades off between IL accuracy and the size of the stability margin of the NN controller. To the best of our knowledge, this is the first attempt to ensure stability of IL based on deep NNs. Second, the stability condition from [8] is nonconvex and thus computationally intractable for NN control synthesis; here we convexify this constraint (using loop transformation) for its efficient enforcement in the learning process. Third, as demonstrated by the numerical example in Section VI-B, while the proposed approach can train a policy that imitates the expert demonstrations, it can potentially improve local stability over suboptimal expert policies, thus enhance the robustness of IL.

Other related works include approximating explicit model predictive control law using NNs for linear parameter varying plant dynamics [13], and LTI plant dynamics [14], [15] to expedite the online evaluation of controllers. Compared with these works, the proposed method provides stability guarantees for the learned NN controller.

The stability and safety issues for learning (especially RL) based control has also been addressed by a Hamilton-Jacobi reachability-based framework in [16], a control barrier function based method in [17], [18], and a convex projection operator based method in [19].

Notation. \mathbb{S}^n , \mathbb{S}_+^n and \mathbb{S}_{++}^n denote the sets of n -by- n symmetric, positive semidefinite and positive definite matrices, respectively. When applied to vectors, the orders $>$, \leq are applied elementwise. For $P \in \mathbb{S}_{++}^n$, define the ellipsoid

$$\mathcal{E}(P) := \{x \in \mathbb{R}^n : x^\top P x \leq 1\}. \quad (1)$$

II. PROBLEM FORMULATION

Consider the feedback system consisting of a plant G and state-feedback controller π as shown in Figure 1. We assume the plant G is a linear, time-invariant (LTI) system defined by the following discrete-time model:

$$x(k+1) = A_G x(k) + B_G u(k), \quad (2)$$

where $x(k) \in \mathbb{R}^{n_G}$ is the state and $u(k) \in \mathbb{R}^{n_u}$ is the control, $A_G \in \mathbb{R}^{n_G \times n_G}$ and $B_G \in \mathbb{R}^{n_G \times n_u}$. Finally, assume $x(k)$ is

constrained to a set $X \subset \mathbb{R}^{n_G}$, which is referred to as the “safety condition”. This state constraint set is assumed to be a polytope symmetric around the origin:

$$X = \{x \in \mathbb{R}^{n_G} : -h \leq Hx \leq h, h \geq 0\}, \quad (3)$$

where $H \in \mathbb{R}^{n_x \times n_G}$, and $h \in \mathbb{R}^{n_x}$. The controller $\pi : \mathbb{R}^{n_G} \rightarrow \mathbb{R}^{n_u}$ is an ℓ -layer, feedforward neural network (NN) defined as:

$$w^0(k) = x(k), \quad (4a)$$

$$w^i(k) = \phi^i (W^i w^{i-1}(k) + b^i), \quad i = 1, \dots, \ell, \quad (4b)$$

$$u(k) = W^{\ell+1} w^\ell(k) + b^{\ell+1}, \quad (4c)$$

where $w^i \in \mathbb{R}^{n_i}$ are the outputs (activations) from the i^{th} layer and $n_0 = n_G$. The operations for each layer are defined by a weight matrix $W^i \in \mathbb{R}^{n_i \times n_{i-1}}$, bias vector $b^i \in \mathbb{R}^{n_i}$, and activation function $\phi^i : \mathbb{R}^{n_i} \rightarrow \mathbb{R}^{n_i}$. The activation function ϕ^i is applied element-wise, i.e.

$$\phi^i(v) := [\varphi(v_1), \dots, \varphi(v_{n_i})]^\top, \quad (5)$$

where $\varphi : \mathbb{R} \rightarrow \mathbb{R}$ is the (scalar) activation function selected for the NN. Common choices for the scalar activation function include tanh, ReLU, and leaky ReLU. We assume the activation φ is identical in all layers; this can be relaxed with minor changes to the notation. We also assume that the activation φ satisfies $\varphi(0) = 0$.

Our goal is to stabilize an equilibrium, which we assume is shifted to the origin as is standard in control design. To ensure that the equilibrium remains at the origin with the NN controller, we impose the constraint $\pi(0) = 0$. Since $\pi(0) = 0$ translates to a nonconvex constraint on (W^i, b^i) , we set all the bias terms to be zero: $b^i = 0_{n_i \times 1}$, for $i = 1, \dots, \ell + 1$.

Remark 1: Setting the bias terms to zero is arguably an underuse of NNs. Whether $\pi(0) = 0$ can be achieved with less restrictive convex constraints is an interesting problem that deserves further research.

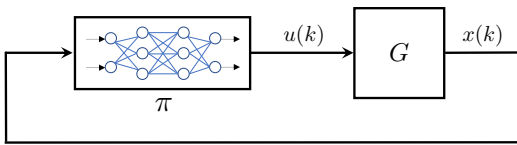


Fig. 1: Feedback system with plant G and NN π

If control constraint sets are hypercubes, they can be considered in the framework by applying activation functions, like tanh, elementwise to the output layer (4c).

Let $\chi(k; x_0)$ denote the solution to the feedback system at time k from initial condition $x(0) = x_0$. The region of attraction (ROA) is defined below.

Definition 1: The region of attraction (ROA) of the feedback system with plant G and NN π is defined as

$$\mathcal{R} := \{x_0 \in X : \lim_{k \rightarrow \infty} \chi(k; x_0) = 0_{n_G \times 1}\}. \quad (6)$$

Given state and control data pairs from the expert demonstrations, our goal is to learn a NN controller from the data to reproduce the demonstrated behavior, while guaranteeing the system trajectories under the control of the learned NN

controller satisfy the safety condition ($x(k) \in X \forall k \geq 0$), and are able to converge to the equilibrium point if they start from the ROA associated with the learned NN controller.

III. STABILITY AND SAFETY CONDITIONS FOR NN CONTROLLED SYSTEMS

In this section, we treat the parameters of the NN controller as fixed and derive the safety and local stability conditions of the NN-controlled LTI systems.

A. NN Representation: Isolation of Nonlinearities

It is useful to isolate the nonlinear activation functions from the linear operations of the NN as done in [5], [20]. Define v^i as the input to the activation function ϕ^i (recalling that $b^i = 0_{n_i \times 1}$ by Remark 1):

$$v^i(k) := W^i w^{i-1}(k), \quad i = 1, \dots, \ell. \quad (7)$$

The nonlinear operation of the i^{th} layer (4b) is thus expressed as $w^i(k) = \phi^i(v^i(k))$. Gather the inputs and outputs of all activation functions:

$$v_\phi := \begin{bmatrix} v^1 \\ \vdots \\ v^\ell \end{bmatrix} \in \mathbb{R}^{n_\phi} \quad \text{and} \quad w_\phi := \begin{bmatrix} w^1 \\ \vdots \\ w^\ell \end{bmatrix} \in \mathbb{R}^{n_\phi}, \quad (8)$$

where $n_\phi := \sum_{i=1}^{\ell} n_i$, and define the combined nonlinearity $\phi : \mathbb{R}^{n_\phi} \rightarrow \mathbb{R}^{n_\phi}$ by stacking the activation functions:

$$\phi(v_\phi) := \begin{bmatrix} \phi^1(v^1) \\ \vdots \\ \phi^\ell(v^\ell) \end{bmatrix}. \quad (9)$$

Thus $w_\phi(k) = \phi(v_\phi(k))$, where the scalar activation function φ is applied element-wise to each entry of v_ϕ . Finally, the NN control policy π defined in (4) can be rewritten as:

$$\begin{bmatrix} u(k) \\ v_\phi(k) \end{bmatrix} = N \begin{bmatrix} x(k) \\ w_\phi(k) \end{bmatrix} \quad (10a)$$

$$w_\phi(k) = \phi(v_\phi(k)). \quad (10b)$$

The matrix N depends on the weights as follows, where the vertical and horizontal bars partition N compatibly with the inputs (x, w_ϕ) and outputs (u, v_ϕ) :

$$N = \left[\begin{array}{c|ccc|c} 0 & 0 & 0 & \dots & w^{\ell+1} \\ w^1 & 0 & \dots & 0 & 0 \\ 0 & w^2 & \dots & 0 & 0 \\ \vdots & \vdots & \vdots & \vdots & \vdots \\ 0 & 0 & \dots & w^\ell & 0 \end{array} \right] := \begin{bmatrix} N_{ux} & N_{uw} \\ N_{vx} & N_{vw} \end{bmatrix}.$$

This decomposition of the NN, depicted in Figure 2, isolates the nonlinearities ϕ in preparation for the stability analysis.

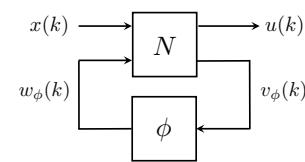


Fig. 2: NN representation to isolate the nonlinearities ϕ .

B. Quadratic Constraints: Scalar Activation Functions

The stability analysis relies on quadratic constraints (QCs) to bound the activation function. A typical constraint is the sector bound as defined next.

Definition 2: Let $\alpha \leq \beta$ be given. The function $\varphi : \mathbb{R} \rightarrow \mathbb{R}$ lies in the (global) sector $[\alpha, \beta]$ if:

$$(\varphi(\nu) - \alpha\nu) \cdot (\beta\nu - \varphi(\nu)) \geq 0 \quad \forall \nu \in \mathbb{R}. \quad (11)$$

The interpretation of the sector $[\alpha, \beta]$ is that φ lies between lines passing through the origin with slope α and β . Many activation functions are bounded in the sector $[0, 1]$, e.g. tanh and ReLU. Figure 3 illustrates $\varphi(\nu) = \tanh(\nu)$ (blue solid) and the global sector defined by $[0, 1]$ (red solid lines).

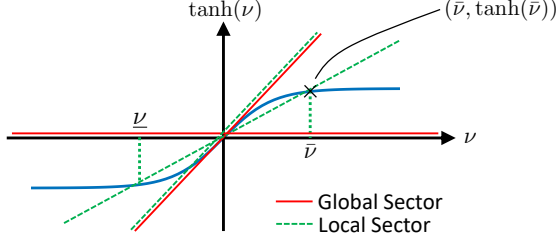


Fig. 3: Sector constraints on tanh

The global sector is often too coarse for analysis; thus, we consider a local sector for tighter bounds.

Definition 3: Let $\alpha, \beta, \underline{\nu}, \bar{\nu} \in \mathbb{R}$ with $\alpha \leq \beta$ and $\underline{\nu} \leq 0 \leq \bar{\nu}$. The function $\varphi : \mathbb{R} \rightarrow \mathbb{R}$ satisfies the local sector $[\alpha, \beta]$ if $(\varphi(\nu) - \alpha\nu) \cdot (\beta\nu - \varphi(\nu)) \geq 0 \quad \forall \nu \in [\underline{\nu}, \bar{\nu}]$.

As an example, $\varphi(\nu) := \tanh(\nu)$ restricted to the interval $[-\bar{\nu}, \bar{\nu}]$ satisfies the local sector bound $[\alpha, \beta]$ with $\alpha := \tanh(\bar{\nu})/\bar{\nu} > 0$ and $\beta := 1$. As shown in Figure 3 (green dashed lines), the local sector provides a tighter bound than the global sector. These bounds are valid for a symmetric interval around the origin with $\underline{\nu} = -\bar{\nu}$; non-symmetric intervals ($\underline{\nu} \neq -\bar{\nu}$) can be handled similarly.

C. Quadratic Constraints: Combined Activation Functions

Local sector constraints can also be defined for the combined nonlinearity ϕ , given by (9). Let $\underline{\nu}, \bar{\nu} \in \mathbb{R}^{n_\phi}$ be given with $\underline{\nu} \leq 0 \leq \bar{\nu}$. Suppose that the activation input $v_\phi \in \mathbb{R}^{n_\phi}$ lies element-wise in the interval $[\underline{\nu}, \bar{\nu}]$ and the i^{th} input/output pair is $w_i = \varphi(v_i)$, and the scalar activation function satisfies the local sector $[\alpha_i, \beta_i]$ with the input restricted to $v_i \in [\underline{\nu}_i, \bar{\nu}_i]$ for $i = 1, \dots, n_\phi$. The local sector bounds can be computed for φ on the given interval analytically (as above for tanh). These local sectors can be stacked into vectors $\alpha_\phi, \beta_\phi \in \mathbb{R}^{n_\phi}$ that provide QCs satisfied by the combined nonlinearity ϕ .

Lemma 1: Let $\alpha_\phi, \beta_\phi, \underline{\nu}, \bar{\nu} \in \mathbb{R}^{n_\phi}$ be given with $\alpha_\phi \leq \beta_\phi$, and $\underline{\nu} \leq 0 \leq \bar{\nu}$. Suppose that ϕ satisfies the local sector $[\alpha_\phi, \beta_\phi]$ element-wise for all $v_\phi \in [\underline{\nu}, \bar{\nu}]$. For any $\lambda \in \mathbb{R}^{n_\phi}$ with $\lambda \geq 0$, and for all $v_\phi \in [\underline{\nu}, \bar{\nu}]$, $w_\phi = \phi(v_\phi)$, it holds

$$\begin{bmatrix} v_\phi \\ w_\phi \end{bmatrix}^\top \begin{bmatrix} -2A_\phi B_\phi \Lambda & (A_\phi + B_\phi) \Lambda \\ (A_\phi + B_\phi) \Lambda & -2\Lambda \end{bmatrix} \begin{bmatrix} v_\phi \\ w_\phi \end{bmatrix} \geq 0, \quad (12)$$

where $A_\phi = \text{diag}(\alpha_\phi)$, $B_\phi = \text{diag}(\beta_\phi)$, and $\Lambda = \text{diag}(\lambda)$.

Proof: The proof can be found in [8, Lemma 1]. ■

In order to apply the local sector bounds in the stability analysis, we must first compute the bounds $\underline{\nu}, \bar{\nu} \in \mathbb{R}^{n_\phi}$ on the activation input v_ϕ . The process to compute the bounds is briefly discussed here with more details provided in [8], [21]. The first step is to find the smallest hypercube that bounds the state constraint set: $X \subseteq \{x : \underline{x} \leq x \leq \bar{x}\}$. Therefore, w^0 (defined in (4a)) is defined by $\underline{w}^0 = \underline{x}$ and $\bar{w}^0 = \bar{x}$. Define $c = \frac{1}{2}(\bar{w}^0 + \underline{w}^0)$, $r = \frac{1}{2}(\bar{w}^0 - \underline{w}^0)$, and denote y^\top as the i^{th} row of W^1 . Then the first activation input $v^1 = W^1 w^0$ is bounded by $[\underline{v}^1, \bar{v}^1]$, where $\bar{v}_i^1 = y^\top c + \sum_{j=1}^{n_0} |y_j r_j|$, and $\underline{v}_i^1 = y^\top c - \sum_{j=1}^{n_0} |y_j r_j|$. If the activation functions ϕ^1 are monotonically non-decreasing, then the first activation output w^1 is bounded by $\underline{w}^1 = \phi^1(\underline{v}^1)$ and $\bar{w}^1 = \phi^1(\bar{v}^1)$. This process can be propagated through all layers of the NN to obtain the bounds $\underline{\nu}, \bar{\nu} \in \mathbb{R}^{n_\phi}$ for the activation input v_ϕ . The remainder of the paper will assume the local sector bounds have been computed as briefly summarized in the following property.

Property 1: Let the state constraint set X and its corresponding activation input bounds $\underline{\nu}, \bar{\nu}$ be given. There exist α_ϕ, β_ϕ such that ϕ satisfies the local sector for all $v_\phi \in [\underline{\nu}, \bar{\nu}]$.

D. Lyapunov Condition

This section uses a Lyapunov function and the local sector to compute an inner approximation for the ROA of the feedback system of G and π .

Theorem 1: ([8]) Consider the feedback system of plant G in (2) and NN π in (4) with equilibrium point $x_* = 0_{n_G \times 1}$, and the state constraint set X . Let $\bar{\nu}, \underline{\nu}, \alpha_\phi, \beta_\phi \in \mathbb{R}^{n_\phi}$ be given vectors satisfying Property 1 for the NN and the set X . Denote the i^{th} row of the matrix H by H_i^\top and define

$$R_V := \begin{bmatrix} I_{n_G} & 0_{n_G \times n_\phi} \\ N_{ux} & N_{uw} \end{bmatrix}, \quad \text{and} \quad R_\phi := \begin{bmatrix} N_{vx} & N_{vw} \\ 0_{n_\phi \times n_G} & I_{n_\phi} \end{bmatrix}.$$

If there exists a matrix $P \in \mathbb{S}_{++}^{n_G}$, and vector $\lambda \in \mathbb{R}^{n_\phi}$ with $\lambda \geq 0$ such that $\Lambda = \text{diag}(\lambda)$ satisfying

$$\begin{aligned} R_V^\top \begin{bmatrix} A_G^\top P A_G - P & A_G^\top P B_G \\ B_G^\top P A_G & B_G^\top P B_G \end{bmatrix} R_V \\ + R_\phi^\top \begin{bmatrix} -2A_\phi B_\phi \Lambda & (A_\phi + B_\phi) \Lambda \\ (A_\phi + B_\phi) \Lambda & -2\Lambda \end{bmatrix} R_\phi < 0, \end{aligned} \quad (13a)$$

$$\begin{bmatrix} h_i^2 & H_i^\top \\ H_i & P \end{bmatrix} \geq 0, \quad i = 1, \dots, n_X, \quad (13b)$$

then: (i) the feedback system consisting of G and π is locally asymptotically stable around x_* , and (ii) the set $\mathcal{E}(P)$, defined by (1), is an inner-approximation to the ROA.

Proof: The proof can be found in [8, Theorem 1]. ■

The Lyapunov condition (13a) is convex in P and λ if the weight matrix N is given, and thus we can efficiently compute the ROA inner-estimates. However, this condition is computationally intractable for NN controller synthesis, as it is nonconvex if we search over N, P , and λ simultaneously.

IV. CONVEX STABILITY AND SAFETY CONDITIONS

In [11], [12], α_ϕ is set to zero to formulate convex constraints. However, this restriction is too coarse for stability analysis of NN controlled systems. Instead, we perform a

loop transformation as shown in Fig. 4 to convexify the stability condition without having restrictions on α_ϕ and β_ϕ .

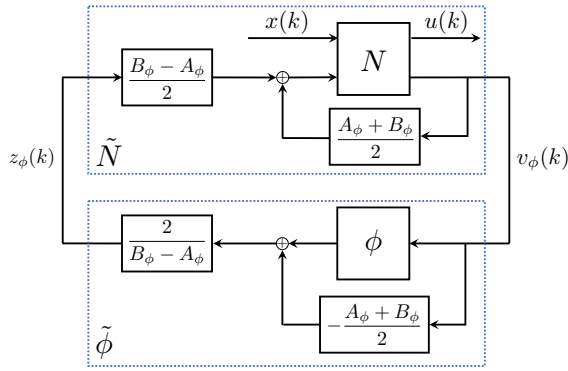


Fig. 4: Loop transformation. If ϕ is in the sector $[\alpha_\phi, \beta_\phi]$, then $\tilde{\phi}$ is in the sector $[-1_{n_\phi \times 1}, 1_{n_\phi \times 1}]$.

A. Loop transformation

Through loop transformation, we obtain a new representation of the NN controller, which is equivalent to (10),

$$\begin{bmatrix} u(k) \\ v_\phi(k) \end{bmatrix} = \tilde{N} \begin{bmatrix} x(k) \\ z_\phi(k) \end{bmatrix}, \quad (14a)$$

$$z_\phi(k) = \tilde{\phi}(v_\phi(k)), \quad (14b)$$

where \tilde{N} and $\tilde{\phi}$ are defined in Fig. 4. Here, we also partition \tilde{N} compatibly with the inputs (x, z_ϕ) and outputs (u, v_ϕ)

$$\tilde{N} = \begin{bmatrix} \tilde{N}_{ux} & \tilde{N}_{uz} \\ \tilde{N}_{vx} & \tilde{N}_{vz} \end{bmatrix}. \quad (15)$$

The loop transformation normalizes the nonlinearity $\tilde{\phi}$ to lie in the sector $[-1_{n_\phi \times 1}, 1_{n_\phi \times 1}]$. As a result, $\tilde{\phi}$ satisfies the sector QC for any $\Lambda = \text{diag}(\lambda)$ with $\lambda \geq 0$:

$$\begin{bmatrix} v_\phi \\ z_\phi \end{bmatrix}^\top \begin{bmatrix} \Lambda & 0 \\ 0 & -\Lambda \end{bmatrix} \begin{bmatrix} v_\phi \\ z_\phi \end{bmatrix} \geq 0, \quad \forall v_\phi \in [\underline{v}, \bar{v}]. \quad (16)$$

The input to N is transformed by the following equation:

$$w_\phi(k) = \frac{B_\phi - A_\phi}{2} z_\phi(k) + \frac{A_\phi + B_\phi}{2} v_\phi(k). \quad (17)$$

The transformed matrix \tilde{N} can be computed by combining this relation with (10a). Substituting (17) into (10a) we obtain

$$u(k) = N_{ux}x(k) + C_1 z_\phi(k) + C_2 v_\phi(k), \quad (18)$$

$$v_\phi(k) = N_{vx}x(k) + C_3 z_\phi(k) + C_4 v_\phi(k), \quad (19)$$

$$\text{where } C_1 = N_{uw} \frac{B_\phi - A_\phi}{2}, \quad C_2 = N_{uw} \frac{A_\phi + B_\phi}{2}, \\ C_3 = N_{vw} \frac{B_\phi - A_\phi}{2}, \quad C_4 = N_{vw} \frac{A_\phi + B_\phi}{2}.$$

The expression for $v_\phi(k)$ can be solved from (19):

$$v_\phi(k) = (I - C_4)^{-1} N_{vx}x(k) + (I - C_4)^{-1} C_3 z_\phi(k). \quad (20)$$

Substituting (20) into (18) yields

$$u(k) = (N_{ux} + C_2(I - C_4)^{-1} N_{vx})x(k) \\ + (C_1 + C_2(I - C_4)^{-1} C_3)z_\phi(k). \quad (21)$$

Matching (20) and (21) with (14a) we get

$$\tilde{N} = \begin{bmatrix} N_{ux} + C_2(I - C_4)^{-1} N_{vx} & C_1 + C_2(I - C_4)^{-1} C_3 \\ (I - C_4)^{-1} N_{vx} & (I - C_4)^{-1} C_3 \end{bmatrix}.$$

Thus, \tilde{N} is a function of N denoted concisely as $\tilde{N} = f(N)$. It is important to note that \tilde{N} depends on N both directly, and also indirectly through its dependence on (A_ϕ, B_ϕ) . Specifically, suppose both N and a hypercube state bound $[\underline{x}, \bar{x}]$ are given. Then \tilde{N} is constructed by: (i) propagating $[\underline{x}, \bar{x}]$ through the NN to compute bounds $[\underline{v}, \bar{v}]$ on the activation inputs, (ii) computing local sector bounds (A_ϕ, B_ϕ) consistent with $[\underline{v}, \bar{v}]$, and (iii) performing the steps in this section to compute \tilde{N} from (N, A_ϕ, B_ϕ) .

B. Stability condition after loop transformation

Similar to the original Lyapunov condition (13a), the new Lyapunov condition for the feedback system of G in (2) and NN in (14) can be written as

$$\tilde{R}_V^\top \begin{bmatrix} A_G^\top P A_G - P & A_G^\top P B_G \\ B_G^\top P A_G & B_G^\top P B_G \end{bmatrix} \tilde{R}_V + \tilde{R}_\phi^\top \begin{bmatrix} \Lambda & 0 \\ 0 & -\Lambda \end{bmatrix} \tilde{R}_\phi < 0, \quad (22)$$

$$\text{where } \tilde{R}_V = \begin{bmatrix} I_{n_G} & 0 \\ \tilde{N}_{ux} & \tilde{N}_{uz} \end{bmatrix}, \quad \text{and } \tilde{R}_\phi = \begin{bmatrix} \tilde{N}_{vx} & \tilde{N}_{vz} \\ 0 & I_{n_\phi} \end{bmatrix}. \quad (23)$$

Lemma 2: Consider the feedback system of G in (2) and NN in (10) with the state constraint set X . If there exist a matrix $P \in \mathbb{S}_{++}^{n_G}$, and vector $\lambda \in \mathbb{R}^{n_\phi}$ with $\lambda \geq 0$ such that (22) (where $\tilde{N} = f(N)$) and (13b) hold, then: (i) the feedback system consisting of G in (2) and NN in (10) is locally asymptotically stable around x_* , and (ii) the set $\mathcal{E}(P)$ is a ROA inner-approximation for it.

Proof: It follows from the assumption that (22) and (13b) hold that the feedback system of G in (2) and NN in (14) is locally asymptotically stable around x_* , and $\mathcal{E}(P)$ is its ROA inner-approximation. Since the representations (10) and (14) of NN are equivalent, the feedback system of G in (2) and NN in (10) is identical to the feedback system of G in (2) and NN in (14). As a result, the feedback system consisting of G in (2) and NN in (10) is locally asymptotically stable around x_* , and the set $\mathcal{E}(P)$ is a ROA inner-approximation for it. ■

The new Lyapunov condition (22) is convex in P and Λ using $\tilde{N} = f(N)$, where N is given. To incorporate the stability condition in the IL process, we will proceed by treating $\tilde{N} \in \mathbb{R}^{(n_u+n_\phi) \times (n_G+n_\phi)}$ as a decision variable along with \tilde{P} and Λ , and try to derive a stability condition that is convex in (P, Λ, \tilde{N}) . Substitute (23) into (22) to obtain

$$\begin{bmatrix} \star \\ \star \end{bmatrix}^\top \begin{bmatrix} P & 0 \\ 0 & \Lambda \end{bmatrix} \begin{bmatrix} A_G + B_G \tilde{N}_{ux} & B_G \tilde{N}_{uz} \\ \tilde{N}_{vx} & \tilde{N}_{vz} \end{bmatrix} - \begin{bmatrix} P & 0 \\ 0 & \Lambda \end{bmatrix} < 0.$$

Applying Schur complements yields the equivalent condition

$$\begin{bmatrix} P & 0 & A_G^\top + \tilde{N}_{ux}^\top B_G^\top & \tilde{N}_{vx}^\top \\ 0 & \Lambda & \tilde{N}_{uz}^\top B_G^\top & \tilde{N}_{vz}^\top \\ A_G + B_G \tilde{N}_{ux} & B_G \tilde{N}_{uz} & P^{-1} & 0 \\ \tilde{N}_{vx} & \tilde{N}_{vz} & 0 & \Lambda^{-1} \end{bmatrix} > 0, \quad (24)$$

and $P > 0$, $\Lambda > 0$. Now (24) is linear in \tilde{N} , but still nonconvex in P and Λ . Multiplying (24) on the left and

right by $\text{diag}(P^{-1}, \Lambda^{-1}, I_{n_G}, I_{n_\phi})$ we obtain

$$\begin{bmatrix} Q_1 & 0 & Q_1 A_G^\top + L_1^\top B_G^\top & L_3^\top \\ 0 & Q_2 & L_2^\top B_G^\top & L_4^\top \\ A_G Q_1 + B_G L_1 & B_G L_2 & Q_1 & 0 \\ L_3 & L_4 & 0 & Q_2 \end{bmatrix} > 0, \quad (25)$$

where $Q_1 = P^{-1} > 0$, $Q_2 = \Lambda^{-1} > 0$, $L_1 = \tilde{N}_{ux} Q_1$, $L_2 = \tilde{N}_{uz} Q_2$, $L_3 = \tilde{N}_{vx} Q_1$, and $L_4 = \tilde{N}_{vz} Q_2$.

The stability condition (25) is convex in the decision variables $(Q_1, Q_2, L_1, \dots, L_4)$, where $Q_1 \in \mathbb{S}_{++}^{n_G}$, $Q_2 \in \mathbb{S}_{++}^{n_\phi}$ and Q_2 is a diagonal matrix, $L_1 \in \mathbb{R}^{n_u \times n_G}$, $L_2 \in \mathbb{R}^{n_u \times n_\phi}$, $L_3 \in \mathbb{R}^{n_\phi \times n_G}$, and $L_4 \in \mathbb{R}^{n_\phi \times n_\phi}$. Variables (P, Λ, \tilde{N}) that satisfy the Lyapunov condition (22) can be recovered using the computed $(Q_1, Q_2, L_1, \dots, L_4)$ through the following equations: $P = Q_1^{-1}$, $\Lambda = Q_2^{-1}$, and

$$\tilde{N} = LQ^{-1}, \quad (26)$$

$$\text{where } Q := \begin{bmatrix} Q_1 & 0 \\ 0 & Q_2 \end{bmatrix}, \text{ and } L := \begin{bmatrix} L_1 & L_2 \\ L_3 & L_4 \end{bmatrix}. \quad (27)$$

Thus, the convex stability condition (25) allows us to search over P , Λ , and \tilde{N} simultaneously.

Moreover, to enforce the safety condition $(x(k) \in X \forall k \geq 0)$ of the system, convex constraints on Q_1 are imposed:

$$H_i^\top Q_1 H_i \leq h_i^2, \quad i = 1, \dots, n_X, \quad (28)$$

which is derived directly from (13b) by Schur complements, and using $Q_1 = P^{-1}$. Again, this ensures $\mathcal{E}(Q_1^{-1}) \subseteq X$.

Denote the LMIs (25), (28) with $Q_1 > 0$ and $Q_2 > 0$ altogether as $\text{LMI}(Q, L) > 0$, which will later be incorporated in the IL process to learn robust NN controllers.

Remark 2: Note that model uncertainties are not considered in the paper. They can be incorporated in (13a) or (22) using integral quadratic constraints (IQCs) as in [8]. However, to derive convex conditions, like (25), only limited types of uncertainties may be incorporated. This in turn will allow for Zames-Falb IQCs to refine the description of activation functions by capturing their slope restrictions.

V. SAFE IMITATION LEARNING ALGORITHM

Given state and control data pairs from the expert demonstrations, we use a loss function $\mathcal{L}(N)$ to train NN controllers with weights N to match the data. Common choices of the loss function include mean squared error, absolute error, and cross-entropy. In general, $\mathcal{L}(N)$ is non-convex in N . We propose the next optimization to solve the safe IL problem,

$$\min_{N, Q, L} \eta_1 \mathcal{L}(N) - \eta_2 \log \det(Q_1) \quad (29a)$$

$$\text{s.t. } \text{LMI}(Q, L) > 0 \quad (29b)$$

$$f(N)Q = L \quad (29c)$$

where Q and L are defined in (27). The optimization has separate objectives. The cost function (29a) combines the IL loss function with a term that attempts to increase the volume of $\mathcal{E}(Q_1^{-1})$ (which is proportional to $\det(Q_1)$). The parameters $\eta_1, \eta_2 > 0$ reflect the relative importance between imitation learning accuracy and size of the robustness margin. The optimization has two sets of decision variables: N and (Q, L) . The former is involved in mimicking the

expert behaviour, and the latter are involved in the stability and safety constraints (29b). The two sets of variables are connected through the equality constraint (29c). Note that (29c) is equivalent to $f(N) = LQ^{-1}$, and the term on the right-hand side equals to \tilde{N} from (26). Therefore, (29c) essentially means that the first set of decision variable N , after being transformed by the nonlinear function f , satisfies the stability and safety constraints.

Similar to [11], we use the alternating direction method of multipliers (ADMM) algorithm to solve this constrained learning problem. We first define an augmented loss function

$$\begin{aligned} \mathcal{L}_a(N, Q, L, Y) = & \eta_1 \mathcal{L}(N) - \eta_2 \log \det(Q_1) \\ & + \text{tr}(Y^\top \cdot (f(N)Q - L)) + \frac{\rho}{2} \|f(N)Q - L\|_F^2, \end{aligned} \quad (30)$$

where $\|\cdot\|_F$ is the Frobenius norm, $Y \in \mathbb{R}^{(n_u + n_\phi) \times (n_G + n_\phi)}$ is the Lagrange multiplier, and $\rho > 0$ is the regularization parameter typically affecting the convergence rate of ADMM. The ADMM algorithm takes the following form:

1. N -update: $N^{k+1} = \arg \min_N \mathcal{L}_a(N, Q^k, L^k, Y^k)$.
2. (Q, L) -update: $(Q, L)^{k+1} = \arg \min_{Q, L} \mathcal{L}_a(N^{k+1}, Q, L, Y^k)$
s.t. $\text{LMI}(Q, L) > 0$
3. Y -update: If $\|f(N^{k+1})Q^{k+1} - L^{k+1}\|_F \leq \sigma$, where $\sigma > 0$ is the stopping tolerance, then the algorithm has converged, and we have found a solution to (29), so terminate the algorithm. Otherwise, update Y and return to step 1.

$$Y^{k+1} = Y^k + \rho (f(N^{k+1})Q^{k+1} - L^{k+1})$$

The unconstrained optimization in Step 1 can be solved using gradient based algorithm. The optimization in Step 2 is convex, and can be solved effectively using SDP solvers. The variable Y in Step 3 accumulates the deviation from the constraint (29c). The individual steps are well-behaved: Gradient descent in Step 1 almost surely converges to local optima [22] and Step 2 always obtains a global optimum. However, the loss $\mathcal{L}(N)$ and constraint (29c) are nonconvex and hence the proposed ADMM does not guarantee convergence to a global optima. Convergence properties of ADMM without convexity are still subject to ongoing research [23]. However, any converged solution provides a safe NN controller with stability and safety guarantees.

In Step 2, Q and L introduce $\mathcal{O}(n_G + n_\phi)$ and $\mathcal{O}((n_G + n_\phi) \times (n_u + n_\phi))$ decision variables. The complexity of primal/dual SDP solvers scales cubically with the number of decision variables. Hence Step 2 will be computationally expensive if the number of activation functions n_ϕ is large.

VI. EXAMPLES

In the following examples, Step 1 in the ADMM algorithm is implemented on Tensorflow, and solved by ADAM [24]. Step 2 is formulated using CVX, and is solved by MOSEK. The mean squared error is chosen as the loss function $\mathcal{L}(N)$. The code is available at <https://github.com/heyinUCB/IQCbasedImitationLearning>

A. Inverted pendulum

Consider an inverted pendulum with mass $m = 0.15$ kg, length $l = 0.5$ m, and friction coefficient $\mu = 0.5$ Nms/rad. The discretized and linearized dynamics are:

$$\begin{bmatrix} x_1(k+1) \\ x_2(k+1) \end{bmatrix} = \begin{bmatrix} 1 & \delta \\ \frac{g\delta}{l} & 1 - \frac{\mu\delta}{ml^2} \end{bmatrix} \begin{bmatrix} x_1(k) \\ x_2(k) \end{bmatrix} + \begin{bmatrix} 0 \\ \frac{\delta}{ml^2} \end{bmatrix} u(k),$$

where the states x_1, x_2 represent the angular position (rad) and velocity (rad/s), u is the control input (Nm), and $\delta = 0.02$ s is the sampling time. The state constraint set is $X = [-2.5, 2.5] \times [-6, 6]$. To generate state and control data pairs for IL, we design an explicit model predictive controller (MPC) to serve as the expert. By fitting a NN controller to the explicit MPC controller, we can expedite the evaluation of controllers during run-time [13]–[15]. In this example, besides a NN controller, we will also provide its associated ROA inner-approximation that guarantees stability and safety. The NN controller is parameterized by a 2-layer, feedforward NN with $n_1 = n_2 = 10$ and tanh as the activation function for both layers. Take $\rho = 1, \eta_1 = 100$, and $\eta_2 = 5$. The ADMM algorithm is terminated after 16 iterations, and $\|f(N) - LQ^{-1}\|_F = 0.17$.

In Fig. 5, the plot on the left shows the learned NN controller with a blue surface, and state and control data pairs from expert demonstrations with orange dots; the plot on the right shows the ROAs of the MPC controller and the NN controller with orange dots and a blue ellipsoid, respectively. We can notice that the ROA of the NN controller is tightly contained by the state constraint set X (shown with a gray rectangle), which guarantees the safety of the system.

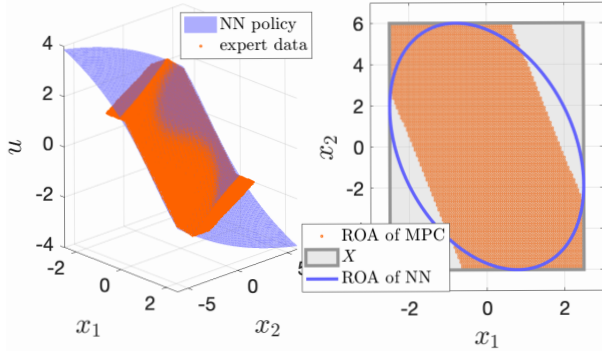


Fig. 5: Left: NN controller vs. expert data from demonstrations; Right: ROAs of MPC controller and NN controller, and state constraint set X of the inverted pendulum

B. Generic Transport Model

The Generic Transport Model (GTM) is a 5.5% scale commercial aircraft. Linearizing and discretizing the longitudinal dynamics given in [25] with sampling time $\delta = 0.02$ s yields:

$$\begin{bmatrix} x_1(k+1) \\ x_2(k+1) \end{bmatrix} = \begin{bmatrix} 0.935 & 0.019 \\ -0.907 & 0.913 \end{bmatrix} \begin{bmatrix} x_1(k) \\ x_2(k) \end{bmatrix} + \begin{bmatrix} -0.006 \\ -1.120 \end{bmatrix} u(k),$$

where the states x_1, x_2 represent angle of attack (rad), and pitch rate (rad/s), and the control u represents the elevator deflection (rad). Take the state constraint set as

$X = [-2, 2] \times [-3, 3]$. In this example, we design an LQR controller to produce expert data. The NN controller is again parameterized by a 2-layer, feedforward NN with $n_1 = n_2 = 16$ and tanh as the activation function for both layers. In this example, we will show how the parameter η_2 affects the result. To do so, two experiments are carried out using two sets of parameters ($\rho = 1, \eta_1 = 100, \eta_2 = 5$) and ($\rho = 1, \eta_1 = 100, \eta_2 = 20$), meaning that we care more about the size of the ROA inner-approximation, and less about the IL accuracy in the second experiment than we do in the first experiment. In both experiments, the ADMM algorithm is terminated in 20 iterations.

The ROA inner-approximations of the NN controllers from the two experiments are shown in Figure 6. The one computed with $\eta_2 = 5$ is shown with a magenta ellipsoid, and the one computed with $\eta_2 = 20$ is shown with a blue ellipsoid. First, it is important to notice that both NN controllers' ROA inner-approximations are larger than that of the expert's LQR controller (shown with a dashed gray ellipsoid), thanks to the second term in the cost function (29a), which enhances the robustness of IL. Also, as expected, the ROA inner-approximation of the NN controller with $\eta_2 = 20$ is larger than that with $\eta_2 = 5$, since a larger η_2 leads to a larger ROA inner-approximation. However, the larger ROA inner-approximation comes at the cost of less accurate regression to the expert data. As shown in Figure 7, the mesh plot of the NN controller with $\eta_2 = 20$ (shown with a blue surface) is more off from the expert data (shown with orange stars) than that with $\eta_2 = 5$ (shown with a magenta surface).

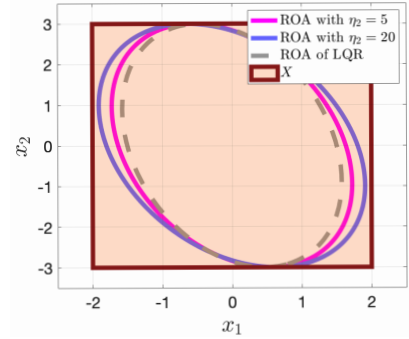


Fig. 6: ROAs and state constraint set X of GTM

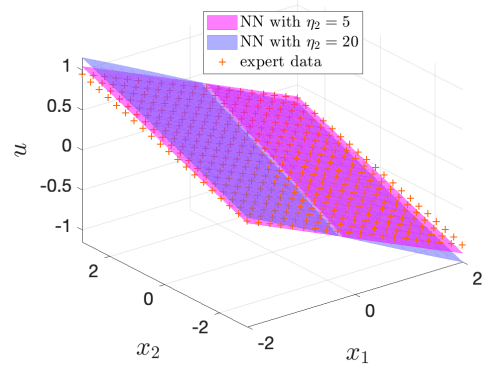


Fig. 7: NN controllers vs. expert data of GTM

C. Vehicle Lateral Control

Consider discretized vehicle lateral dynamics from [8, Eqn 34] with sampling time $\delta = 0.02s$, and a constant curvature $c \equiv 0$. Let $x = [e, \dot{e}, e_\theta, \dot{e}_\theta]$ denote the plant state, where e is the perpendicular distance to the lane edge (m), and e_θ is the angle between the tangent to the straight section of the road and the projection of the vehicle's longitudinal axis (rad). The control u is the steering angle of the front wheel (rad). The state constraint set is $X = [-2, 2] \times [-5, 5] \times [-1, 1] \times [5, 5]$. We design an explicit MPC law to serve as the expert, which is computed with an input constraint $u(k) \in [-\pi/6, \pi/6]$ and a 5-step prediction horizon. The NN controller is parameterized by a 2-layer NN with $n_1 = n_2 = 10$ and \tanh as the activation function for both layers. We perform two experiments using two sets of parameters ($\rho = 1000, \eta_1 = 100, \eta_2 = 100$) and ($\rho = 1000, \eta_1 = 100, \eta_2 = 500$). In both experiments, the ADMM algorithm is terminated in 20 iterations, and the achieved $\|f(N) - LQ^{-1}\|_F$ are 0.14 and 0.08.

As shown in Fig. 8, the ROAs of the NN controllers with $\eta_2 = 100$ and $\eta_2 = 500$ are contained by the state constraint set X shown with maroon boxes, guaranteeing the safety of the system. As expected, the volume of the ROA with $\eta_2 = 500$ is larger than that with $\eta_2 = 100$, and the achieved $\det(Q_1)$ for $\eta_2 = 100$ and $\eta_2 = 500$ are 543 and 663. However, the larger ROA comes at the cost of less accurate regression to the expert data. As shown in Fig. 9, the simulated state and control signals with $\eta_2 = 100$ are closer to those of the MPC law than those with $\eta_2 = 500$.

It takes 0.011 and 0.012 second to run the simulations for the NN controllers for 500 time steps with $\eta_2 = 100$ and $\eta_2 = 500$ on a laptop with an Intel core i5 processor, and it takes 0.38 second for the explicit MPC law, which demonstrates the run-time advantage of NNs over explicit MPC laws.

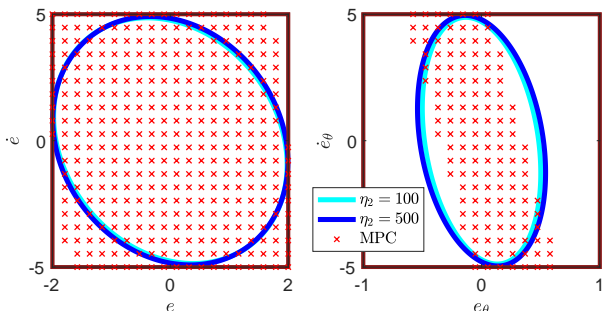


Fig. 8: ROAs of the explicit MPC law (red crosses), and the NN controllers with $\eta_2 = 100$ (cyan curves) and $\eta_2 = 500$ (blue curves)

VII. CONCLUSIONS

In this paper, we present an IL algorithm with stability and safety guarantees. First, we derive convex stability and safety conditions for NN controlled systems. Then, we incorporate these conditions in the IL process, which trades off between the IL accuracy, and the size of the ROA. Finally, we propose an ADMM based algorithm to solve the safe IL problem.

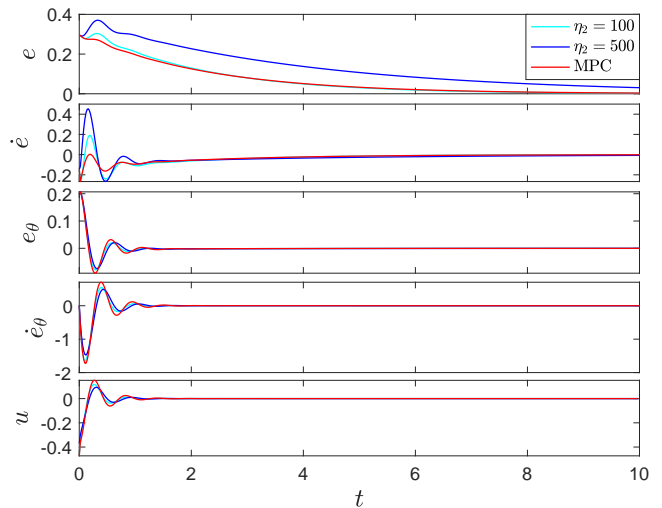


Fig. 9: Simulated signals using the explicit MPC law (red curves), and the NN controllers with $\eta_2 = 100$ (cyan curves) and $\eta_2 = 500$ (blue curves)

REFERENCES

- [1] T. Osa, J. Pajarinen, G. Neumann, J. Bagnell, P. Abbeel, and J. Peters, "An algorithmic perspective on imitation learning," *Foundations and Trends in Robotics*, vol. 7, no. 1-2, pp. 1–179, 2018.
- [2] D. A. Pomerleau, *ALVINN: An Autonomous Land Vehicle in a Neural Network*. San Francisco, CA, USA: Morgan Kaufmann Publishers Inc., 1989, p. 305–313.
- [3] W. Sun, A. Venkatraman, G. J. Gordon, B. Boots, and J. A. Bagnell, "Deeply aggregated: Differentiable imitation learning for sequential prediction," in *International Conference on Machine Learning*, 2017.
- [4] H. Daumé, J. Langford, and D. Marcu, "Search-based structured prediction," *Machine learning*, vol. 75, no. 3, pp. 297–325, 2009.
- [5] M. Fazlyab, M. Morari, and G. J. Pappas, "Safety Verification and Robustness Analysis of Neural Networks via Quadratic Constraints and Semidefinite Programming," p. arXiv:1903.01287, Mar. 2019.
- [6] M. Fazlyab, A. Robey, H. Hassani, M. Morari, and G. Pappas, "Efficient and accurate estimation of Lipschitz constants for deep neural networks," in *Advances in Neural Information Processing Systems 32*. Curran Associates, Inc., 2019, pp. 11 427–11 438.
- [7] H. Hu, M. Fazlyab, M. Morari, and G. J. Pappas, "Reach-SDP: Reachability Analysis of Closed-Loop Systems with Neural Network Controllers via Semidefinite Programming," p. arXiv:2004.07876.
- [8] H. Yin, P. Seiler, and M. Arcak, "Stability Analysis using Quadratic Constraints for Systems with Neural Network Controllers," p. arXiv:2006.07579, Jun. 2020.
- [9] P. Pauli, J. Köhler, J. Berberich, A. Koch, and F. Allgöwer, "Offset-free setpoint tracking using neural network controllers," *arXiv preprint arXiv:2011.14006*, 2020.
- [10] M. Jin and J. Lavaei, "Stability-certified reinforcement learning: A control-theoretic perspective," *arXiv preprint arXiv:1810.11505*, 2018.
- [11] P. Pauli, A. Koch, J. Berberich, and F. Allgöwer, "Training robust neural networks using Lipschitz bounds," p. arXiv:2005.02929.
- [12] M. Revay, R. Wang, and I. R. Manchester, "Convex sets of robust recurrent neural networks," *arXiv preprint arXiv:2004.05290*, 2020.
- [13] X. Zhang, M. Bujarbaruah, and F. Borrelli, "Safe and near-optimal policy learning for model predictive control using primal-dual neural networks," in *2019 American Control Conference (ACC)*, 2019.
- [14] B. Karg and S. Lucia, "Efficient representation and approximation of model predictive control laws via deep learning," *IEEE Transactions on Cybernetics*, vol. 50, no. 9, pp. 3866–3878, 2020.
- [15] S. Chen, K. Saulnier, N. Atanasov, D. D. Lee, V. Kumar, G. J. Pappas, and M. Morari, "Approximating explicit model predictive control using constrained neural networks," in *2018 Annual American Control Conference (ACC)*, 2018, pp. 1520–1527.

- [16] J. F. Fisac, A. K. Akametalu, M. N. Zeilinger, S. Kaynama, J. Gillula, and C. J. Tomlin, "A general safety framework for learning-based control in uncertain robotic systems," *IEEE Transactions on Automatic Control*, vol. 64, no. 7, pp. 2737–2752, 2018.
- [17] A. J. Taylor, A. Singletary, Y. Yue, and A. D. Ames, "A control barrier perspective on episodic learning via projection-to-state safety," *arXiv preprint arXiv:2003.08028*, 2020.
- [18] L. Lindemann, H. Hu, A. Robey, H. Zhang, D. V. Dimarogonas, S. Tu, and N. Matni, "Learning hybrid control barrier functions from data," *arXiv preprint arXiv:2011.04112*, 2020.
- [19] P. L. Donti, M. Roderick, M. Fazlyab, and J. Z. Kolter, "Enforcing robust control guarantees within neural network policies," *arXiv preprint arXiv:2011.08105*, 2020.
- [20] K. K. Kim, E. R. Patrón, and R. D. Braatz, "Standard representation and unified stability analysis for dynamic artificial neural network models," *Neural Networks*, vol. 98, pp. 251–262, 2018.
- [21] S. Gowal, K. Dvijotham, R. Stanforth, R. Bunel, C. Qin, J. Uesato, R. Arandjelovic, T. Mann, and P. Kohli, "On the Effectiveness of Interval Bound Propagation for Training Verifiably Robust Models," p. arXiv:1810.12715, Oct. 2018.
- [22] J. D. Lee, M. Simchowitz, M. I. Jordan, and B. Recht, "Gradient descent only converges to minimizers," in *29th Annual Conference on Learning Theory*, vol. 49. PMLR, 23–26 Jun 2016, pp. 1246–1257.
- [23] Y. Wang, W. Yin, and J. Zeng, "Global convergence of ADMM in nonconvex nonsmooth optimization," *Journal of Scientific Computing*, vol. 78, no. 1, pp. 29–63, 2019.
- [24] D. P. Kingma and J. Ba, "Adam: A method for stochastic optimization," *arXiv preprint arXiv:1412.6980*, 2014.
- [25] A. Chakraborty, P. Seiler, and G. J. Balas, "Nonlinear region of attraction analysis for flight control verification and validation," *Control Engineering Practice*, vol. 19, no. 4, pp. 335–345, 2011.